Correlation between materials and band-selective detection in organic photodetectors based on bulk heterojunction

Quentin Eynaud, Anass Khodr, Mohamed El Amine Kramdi, Gilles Quéléver, Olivier Margeat, Jörg Ackermann, Christine Videlot-Ackermann

▶ **To cite this version:**

Quentin Eynaud, Anass Khodr, Mohamed El Amine Kramdi, Gilles Quéléver, Olivier Margeat, et al.. Correlation between materials and band-selective detection in organic photodetectors based on bulk heterojunction. Journal of Applied Polymer Science, 2024, 10.1002/app.55481 . hal-04519242

HAL Id: hal-04519242
https://hal.science/hal-04519242v1

Submitted on 1 Apr 2024

HAL is a multi-disciplinary open access archive for the deposit and dissemination of scientific research documents, whether they are published or not. The documents may come from teaching and research institutions in France or abroad, or from public or private research centers.

L'archive ouverte pluridisciplinaire **HAL**, est destinée au dépôt et à la diffusion de documents scientifiques de niveau recherche, publiés ou non, émanant des établissements d'enseignement et de recherche français ou étrangers, des laboratoires publics ou privés.

Distributed under a Creative Commons Attribution 4.0 International License

Check for updates

Received: 23 January 2024 | Revised: 6 March 2024 | Accepted: 10 March 2024

DOI: 10.1002/app.55481

RESEARCH ARTICLE

Applied Polymer SCIENCE WILEY

Correlation between materials and band-selective detection in organic photodetectors based on bulk heterojunction

Quentin Eynaud | **Anass Khodr** | **Mohamed El Amine Kramdi** | **Gilles Quéléver** | **Olivier Margeat** | **Jörg Ackermann** | **Christine Videlot-Ackermann**

CNRS, CINaM, Aix Marseille Univ, Marseille, France

Correspondence
Christine Videlot-Ackermann, CNRS, CINaM, Aix Marseille Univ, Marseille, France.
Email: christine.videlot-ackermann@cnrs.fr

Funding information
Agence Nationale de la Recherche, Grant/Award Numbers: ANR-18-CE04-0007-04, ANR-22-CE06-0018

Abstract

For wavelength-selective photodetection or color discrimination, organic photodetectors (OPDs) can provide significant advantages as solution processability, chemical versatility and functionality. To eliminate the need for commonly used filters, the development of a narrowing approach that simultaneously achieves a selective detection range of less than 50 nm bandwidth and a spectral response of ~20% as efficiency at a required wavelength, remains a real challenge. Herein, different donor polymers and small acceptor molecules have been involved in bulk heterojunctions (BHJs) at 1:1 weight ratio as photoactive layers in specific OPDs. Indeed, the mechanism of charge collection in these OPDs is based on the charge collection narrowing (CCN) principle. In this approach, the detection window can be selected to match the absorption onset of the junction materials used in the BHJ layer. Although essentially based on very thick layers, we are focusing here on OPDs with layer thicknesses of less than 2 μm and post-deposition annealing temperatures not in excess of 100°C.

KEYWORDS

blends, optical and photovoltaic applications, optical properties

1 | INTRODUCTION

Spectrally selective photodetection has been largely employed in biomedical monitoring, artificial intelligence imaging, and surveillance, where only band-specific optical signals are intended to be detected.[1] Organic semiconductors have a wide range of properties that make them ideally suited to narrowband photodetection. Recently, several studies demonstrate the possibility to access to filter-free narrowband photodetection by using organic photodetectors (OPDs).[2] OPDs are photodiode type (PD-OPDs) with external quantum efficiency (EQE) less than 100% or photomultiplication type (PM-OPDs) with EQE higher than 100%. To achieve selected color discrimination excluding the use of a filter, different mechanisms have been implemented such as charge collection narrowing (CCN).[3] The CCN mechanism is a new way of controlling the spectral response, with a special feature in that the detection window can be selected to match the absorption onset of the junction materials. Such as solar cells, solution-processable bulk heterojunctions (BHJs) have been applied to achieve high-efficiency CCN-based OPDs. Indeed, BHJ overcome the limitations of the short exciton diffusion length in organic materials

This is an open access article under the terms of the Creative Commons Attribution License, which permits use, distribution and reproduction in any medium, provided the original work is properly cited.
© 2024 The Authors. *Journal of Applied Polymer Science* published by Wiley Periodicals LLC.

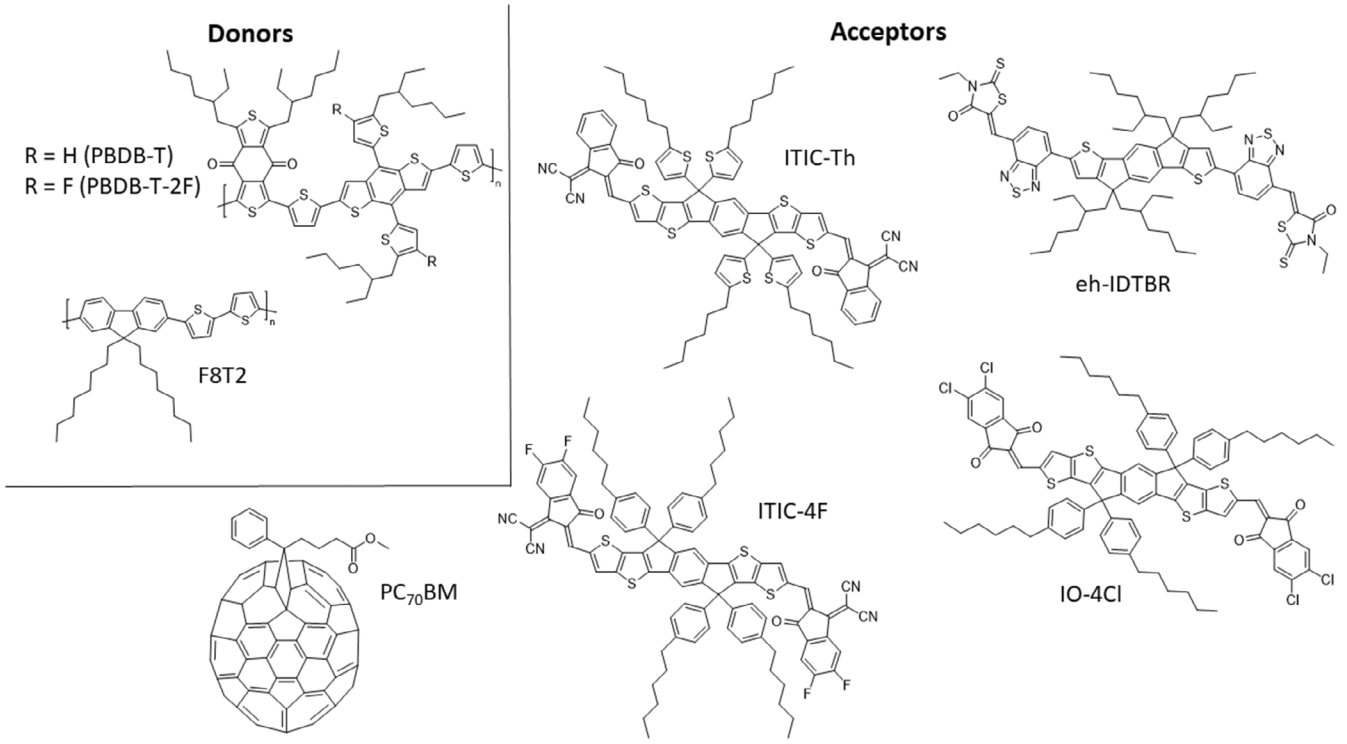

FIGURE 1 Chemical structure of materials.

(≈ 10 nm) and result in greater benefit of incident photons absorption to obtain narrowband OPDs.

Since the first development of high-performance CCN-based OPDs in 2015 by Armin et al.,[3a] divers PD-type OPDs based on donor:acceptor (D:A) BHJs with fullerenes or non-fullerene acceptors (NFAs) as acceptors following the CCN concept have been reported.[3e] The special feature of these OPDs is that they fail to detect the visible light due to their high opacity at these wavelengths. They are referred to as blind to visible light, without the need for additional input filtering to provide a narrow selective peak with a full width at half maximum (FWHM) of less than 100 nm. The detection window can be adjusted according to the absorption onset of the BHJ material system used, while the opacity property outside this spectral detection window will be mainly controlled by the layer thickness. As a result, the CCN concept is highly dependent on the absorption range of the active layer and its thickness. The metric indicators of high efficient narrowband CCN-OPDs are the efficiency (EQE) and the spectral bandwidth (FWHM) of the selective detection peak together with the spectral rejection ratio (SRR) defined as the ratio of the responsivity at the target wavelength to the one at the untargeted reference wavelength (usually in the visible range).

Thanks to the wide variety of materials commonly used in BHJs, both as donor polymers or small molecule acceptors, it is possible to target a large number of detection panels. In recent years, the rise of NFAs resulted in quick development of molecules such as ITIC and IDTBR families (e.g., see Figure 1 for chemical structures of ITIC-Th, ITIC-4F and eh-IDTBR and SI for chemical names). The absorption spectra of NFAs have the great advantage, compared to those of fullerenes, to extend towards the red even near infrared and can be complementary to those of the polymer donors. By the development of these new materials, a wider range of organic molecules is available for these applications, and hence for OPDs. Indeed, by simply changing one of the two materials, the donor polymer or the acceptor, a new BHJ with its own absorption spectrum is formed. However, the simultaneous achievement of high EQE, low FWHM and high SRR is only very exceptionally achieved in the literature with BHJ-based OPDs to follow the CCN principle.[3e] In addition, requirements such as ultra-thick layer and high processing temperatures are often required to manufacture the organic layers to achieve CCN-based OPDs. However, for applications in industry and everyday life such as environmental monitoring, biomedical imaging, surveillance, machine vision and sensing, PD-type OPDs based on the CCN concept have to overcome these constraints, such as an active organic layer thickness of less than 2 μm and post-deposition annealing temperatures not in excess of 100°C.

Here we discuss relevant trends, highlighting the direct correlation between BHJ absorption range and EQE profile to assist in the development of a selective detection peak with a bandwidth of less than 50 nm, a

10974628, 0, Downloaded from https://onlinelibrary.wiley.com/doi/10.1002/app.55481 by Cochrane France, Wiley Online Library on [23/03/2024]. See the Terms and Conditions (https://onlinelibrary.wiley.com/terms-and-conditions) on Wiley Online Library for rules of use; OA articles are governed by the applicable Creative Commons License

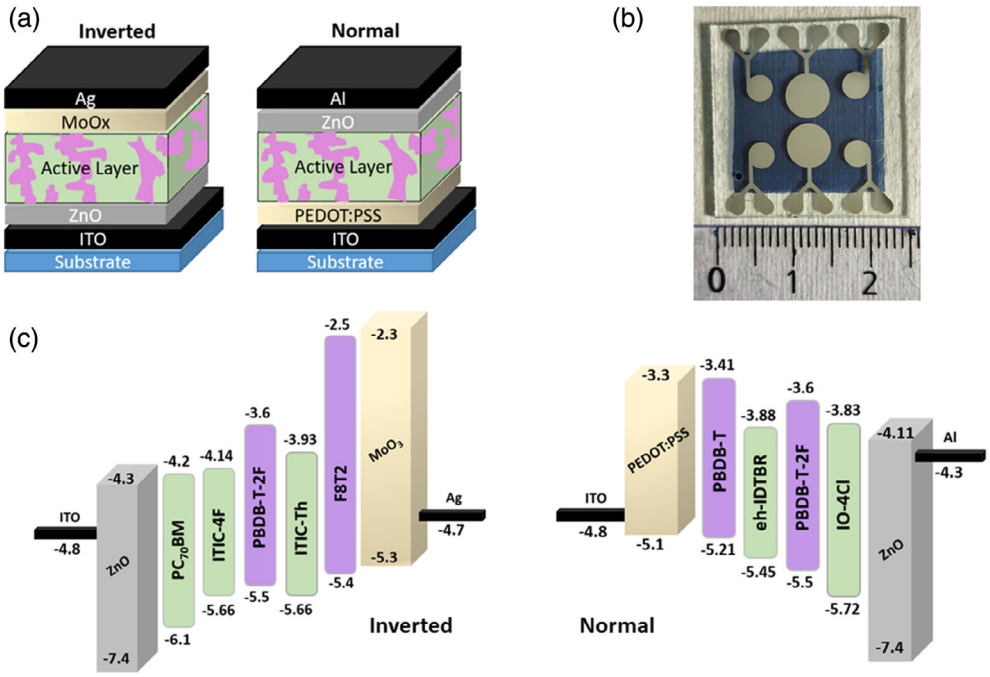

FIGURE 2 Schematic diagram of the inverted and normal structures (a), photograph of devices in normal structure (b) and energy diagram of blend-based OPDs in inverted and normal structures (c). [Color figure can be viewed at wileyonlinelibrary.com]

spectral response of ~20% at low applied bias and a SRR greater than 100. We show here that it is not obvious to combine these three metric parameters while avoiding the constraints of thickness and annealing temperature of organic layers. BHJs based on the mixture between donor polymer and electron acceptor at 1:1 weight ratio (see Figure 1 for chemical structures and SI for chemical names) have been deposited as active layers in OPDs. Devices were fabricated in an inverted or normal structure (Figure 2a). A photograph of devices in normal structure is shown Figure 2b. The energy-level diagrams of the photoactive material are depicted in Figure 2c, showing an ideal band structure of the BHJ films for efficient charge carrier generation and collection.

2 | EXPERIMENTAL SECTION

2.1 | Materials

Patterned ITO substrates (size 25 mm × 25 mm) with 15 Ω/sq resistance were purchased from Lumtec, Taiwan. For normal structure, ZnO nanoparticle ink was prepared as published previously,[4] while for inverted structure a 2.5%vol. ZnO nanoparticle solution in alcohol blend ZnO was purchased from Avantama and diluted to 1% vol. before use. O-xylene, 1,2,3,4-tetrahydronaphthalene (Tetralin), and molybdenum (VI) oxide (MoO_3 purity 99.97%) were purchased from Sigma-Aldrich. PBDB-T, PBDB-T-2F, ITIC-Th, ITIC-4F, eh-IDTBR and IO-4Cl were purchased from 1-Material. PEDOT:PSS (Al 4083) and F8T2 were purchased from Ossila. $PC_{70}BM$ was purchased from Nano-C. Aluminum (Al, purity 99.999%) and silver (Ag, purity 99.99%) were purchased from Kurt J. Lesker. All commercial materials were used as received without purification and kept under nitrogen atmosphere.

2.2 | OPDs fabrication

The photodetectors were fabricated in both normal (ITO/PEDOT:PSS/BHJ/ZnO/Al) and inverted (ITO/ZnO/BHJ/MoO_3/Ag) structures on ITO-coated glasses using spin-coating technique in glove box under nitrogen atmosphere. First, the ITO substrates were thoroughly cleaned with clean cloth dampened with isopropanol before sonication in isopropanol for 30 min and applying UV ozone for 15 min at 80°C. For normal architecture, a thin layer of PEDOT:PSS with thickness of 40 nm was spin-coated on cleaned ITO substrates at 3500 rpm for 60 s, followed by an annealing step at 120°C for 15 min to remove residual solvent from the layer. After BHJ deposition, and to complete devices, 30 nm of ZnO was spin-coated at 2000 rpm for 60 s before annealing at 100°C for 180 s and Al was thermally evaporated to an electrode thickness of 100 nm under a vacuum of 2×10^{-6} mbar through a shadow mask to obtain device areas of 0.09 and 0.25 cm^2. For inverted architecture, a thin layer of ZnO was spin-coated on the cleaned ITO substrate in the ambient conditions at a speed of 5000 rpm for 60 s followed by an annealing step inside nitrogen-filled glove box at 100°C for 10 min to form 15 nm thick film. After BHJ

10974628, 0, Downloaded from https://onlinelibrary.wiley.com/doi/10.1002/app.55481 by Cochrane France, Wiley Online Library on [23/03/2024]. See the Terms and Conditions (https://onlinelibrary.wiley.com/terms-and-conditions) on Wiley Online Library for rules of use; OA articles are governed by the applicable Creative Commons License

deposition, MoO_3 and Ag were successively thermally evaporated at 2×10^{-6} mbar to 2 nm and 100 nm thick layers respectively using a shadow mask to obtain device areas of 0.09 and 0.25 cm^2 (see Figure 2b).

BHJ solutions were prepared in (95% volume) o-xylene and (5% volume) Tetralin at 1:1 weight ratio to a final concentration C (in $mg.mL^{-1}$). Inks have been stirred at a temperature T (in °C) overnight. BHJ layers were spin-coated inside nitrogen-filled glove box at speed v (in rpm) for 120 s following by a post-deposition thermal annealing at 100°C for 10 min to remove residual solvent from layers. (C/T/v for BHJ layer: PBDB-T-2F:ITIC-4F with 38/50/500, PBDB-T-2F:$PC_{70}BM$ with 30-40/80/800, PBDB-T-2F:IO-4Cl with 60/85/1000, PBDB-T: eh-IDTBR with 30/85/1000, F8T2:ITIC-Th with 30/85/3000).

2.3 | Characterization of organic films and OPDs

The absorbance of the active layer films was measured by UV–Vis-near infrared Spectrophotometer Cary 5000. Film thicknesses were measured by a stylus profilometer (Bruker DEKTAK XT) with 1 mg force on the probing tip. EQE measurements were processed in a dark room in ambient conditions with a 150 W Xe arc lamp Apex illuminator (70525) light source collimated to a Cornerstone™ 260 1/4 m UV–VIS Monochromator (74125) from Oriel Instruments for the light part and with a Keithley 238 Source Measure Unit for the electrical part. Devices were mounted on an optical table in a Faraday cage with an aperture to expose the samples to the monochromatic light. The electrodes of the devices were electrically connected to the cage by spring loaded pogo pin connectors. The light beam was filtrated with 295 nm (10CGA-295) and 570 nm (10CGA-570) long-pass filters before reaching the devices.

The responsivity $\mathfrak{R}$ is calculated from the external quantum efficiency (EQE) spectra, using the following equation:

$$\mathfrak{R} = \frac{J_{ph} - J_d}{L_{opt(\lambda)}} \approx \frac{J_{ph}}{L_{opt(\lambda)}} = EQE.\frac{\lambda q}{hc}, \quad (1)$$

where J_{ph} is the current density under illumination, in $mA.cm^{-2}$, L_{opt} is the incident light power density, in $mW.cm^{-2}$. J_d is the dark current density and is extremely small as compared to J_{ph} and therefore can be neglected.[5] λ is the wavelength, q is the electron charge, h is the Planck's constant and c is the speed of light.

OPDs in line with the CCN concept must not detect certain wavelengths while selectively detecting other wavelengths. Nevertheless, the appearance of spurious detections in the area where OPD must be blind (no detection) can create crosstalk. The crosstalk of the OPD over different spectral regions can be described using the spectral rejection ratio (SRR), defined as the ratio of the responsivity at the target wavelength (λ_{target}) to the one at the untargeted wavelength ($\lambda_{untarget}$). SRR can be calculated by:

$$SRR = \frac{\mathfrak{R}(\lambda_{target})}{\mathfrak{R}(\lambda_{untarget})}. \quad (2)$$

Both responsivity values at λ_{target} and at $\lambda_{untarget}$ are specific to the spectral response measured. Each donor:acceptor BHJ will give a spectral response specific to the materials involved in the blend. It will therefore be necessary to identify for each blend, λ_{target} and at $\lambda_{untarget}$. λ_{target} is the wavelength at which $\mathfrak{R}$ is maximal, and $\lambda_{untarget}$ is the wavelength where $\mathfrak{R}$ is supposed to be minimal or even zero, but where spurious detection can be measured. In the present study, $\lambda_{untarget} = 460$ nm for PBDB-T-2F:$PC_{70}BM$, PBDB-T: eh-IDTBR, PBDB-T-2F: ITIC-4F and PBDB-T-2F:IO-4Cl or 532 nm for F8T2: ITIC-Th.

3 | RESULTS AND DISCUSSION

3.1 | Impact of active layer materials on absorption spectra

At first, we investigated the optical properties of blends in thin films spin-coated from o-xylene/tetralin (95/5% in volume), followed by post-deposition thermal annealing at 100°C for 10 min. In order to visualize the contribution of each materials, absorption spectra of neat materials spin-coated from o-xylene/tetralin (95/5% in volume) and subjected to the same post-deposition thermal annealing at 100°C for 10 min are depicted in Figure 3. The maximum absorption wavelengths (λ_{max}) together with the most prominent peaks are summarized in Table S1. For each BHJ, the absorption spectrum corresponds to the addition of the two spectra of single layers. The only exception being IO-4Cl where its absorption spectrum overlaps with that of the PBDB-T-2F donor polymer (see Figure 3e), and will be examined separately in the following. While $PC_{70}BM$ demonstrates a strong light absorption in the UV range with a continuously decrease up to 700 nm in the visible, the absorption of NFA materials is located in the UV–visible region with a maximum from 630 nm for IO-4Cl to 725 nm for ITIC-4F. Upon blending with NFAs, BHJ-based films revealed red shift of absorption compared to $PC_{70}BM$, resulting in shifts of onset absorption wavelengths (λ_{onset}) above 730 nm (Table S1). λ_{onset} is defined as the x-intercept of a tangent line

10974628, 0, Downloaded from https://onlinelibrary.wiley.com/doi/10.1002/app.55481 by Cochrane France, Wiley Online Library on [23/03/2024]. See the Terms and Conditions (https://onlinelibrary.wiley.com/terms-and-conditions) on Wiley Online Library for rules of use; OA articles are governed by the applicable Creative Commons License

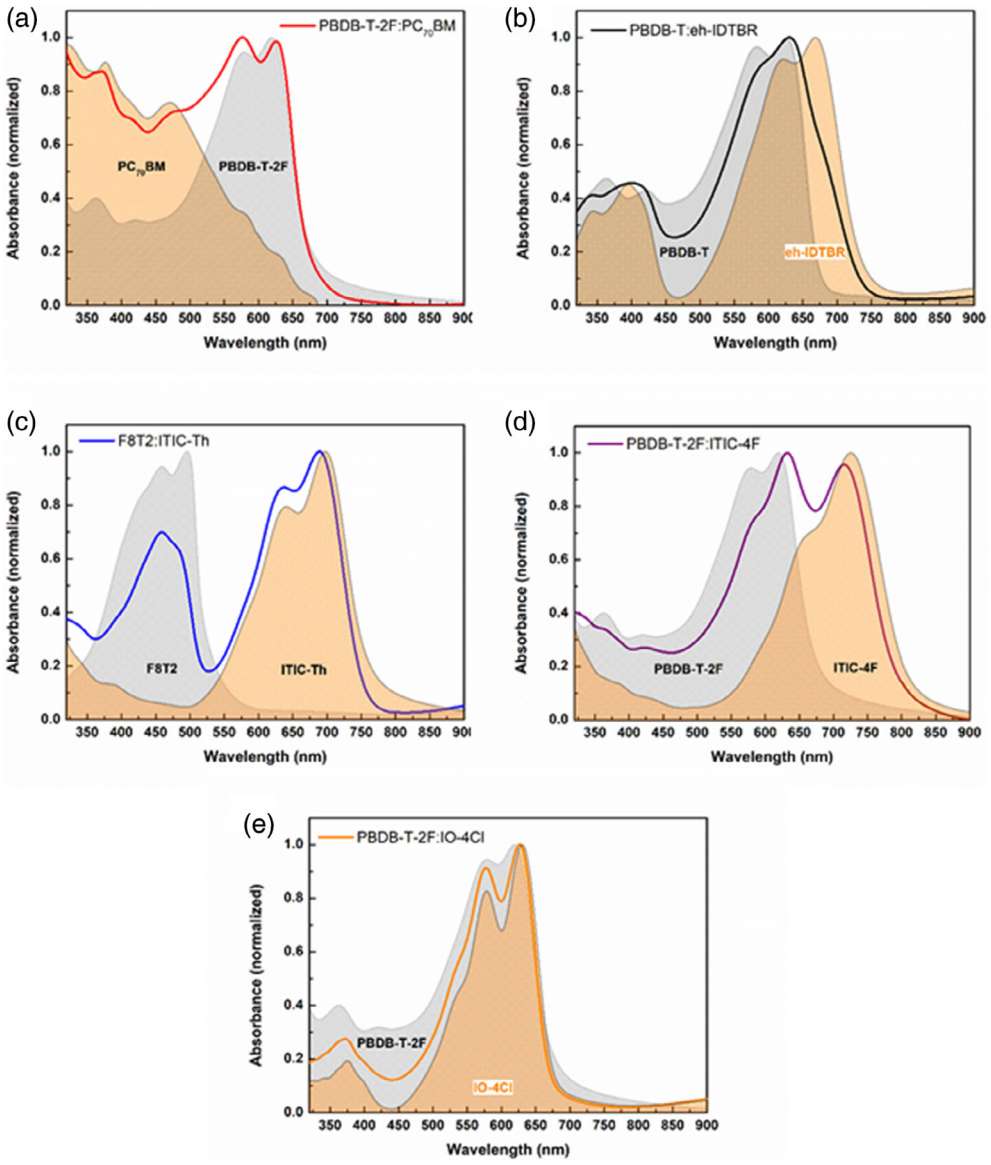

FIGURE 3 Normalized UV–Vis absorption spectra of neat materials (donor in gray and acceptor in orange) and corresponding blended films thermal annealed at 100°C for 10 min. [Color figure can be viewed at wileyonlinelibrary.com]

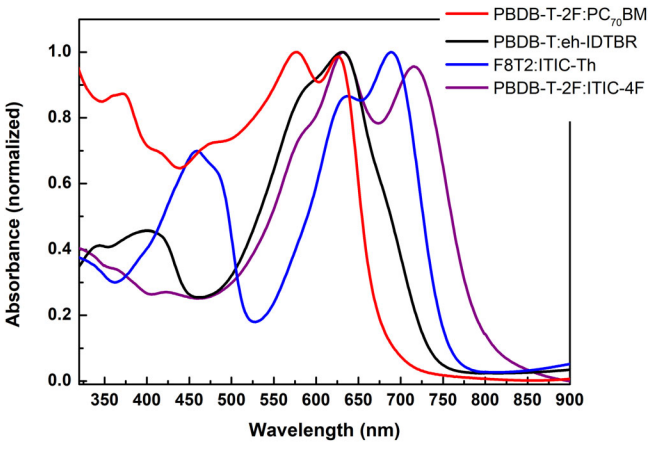

FIGURE 4 Normalized UV–Vis absorption spectra of blended films. [Color figure can be viewed at wileyonlinelibrary.com]

(or line of best fit) on the inflection point for the lowest energy absorption transition of blends, and generally corresponds to the expected active detection window of BHJ-based OPDs in order to respect the CCN principle (see Figure S1).

The normalized ultraviolet–visible (UV–vis) optical absorption spectra of PBDB-T-2F:$PC_{70}BM$, PBDB-T: eh-IDTBR, F8T2:ITIC-Th and PBDB-T-2F:ITIC-4F based thin films (ratio 1:1) are shown in Figure 4.

3.2 | Impact of film thickness for wavelength-selective photodetection

Bi-continuous interpenetrating network morphology formed spontaneously in most BHJ layers is highly

10974628, 0, Downloaded from https://onlinelibrary.wiley.com/doi/10.1002/app.55481 by Cochrane France, Wiley Online Library on [23/03/2024]. See the Terms and Conditions (https://onlinelibrary.wiley.com/terms-and-conditions) on Wiley Online Library for rules of use; OA articles are governed by the applicable Creative Commons License

desirable for OPDs. In order to strengthen this ideal morphology and to suppress unfavorable phase separation domains or isolated aggregation regions, the presence of additives to BHJ solutions in o-xylene, in our case 5% by volume of Tetralin, is recommended. In a previous detailed study, we demonstrated by GIWAXS and Raman that thick PBDB-T-2F:ITIC-4F blends are bi-continuous interpenetrating networks suitable for modeling as a single effective medium.[3d] However, there is fundamental differences between thin (a few hundred nm thick) and thick (thickness greater than 1 μm) films. For thin BHJs, photon absorption and charge carrier distribution across the active layer at 1 sun (with 1 sun = 100 mW cm^{-2} under simulated AM1.5G solar spectrum irradiance) are relatively homogeneous, which is no longer the case for thick films. The operating principle of OPDs is based on electrical responses by converting photons into charge carriers and producing a change in voltage or current in electrical circuits. The spectral response of OPDs is highly dependent on the efficiency of each step leading to charge collection, namely photon harvesting, exciton dissociation, creation, transport and collection of charge carriers. In layers of micrometric thickness, this response will be all the more unusual in because the layers are opaque at some lengths, so photons will not be able to be absorbed and take part in the creation and collection of charge carriers. Without charge creation at these wavelengths, the contribution to conversion is therefore nonexistent, resulting in an ideal EQE of zero.

To investigate the evolution of spectra as a function of active layer thickness, Figure 5 shows EQE spectra at zero bias (0 V) of PD-type OPDs based on PBDB-T-2F:ITIC-4F in 1:1 ratio post-annealed at 100°C or 200°C with active layer thicknesses ranging from 225 to 3310 nm. At 100°C for thinner layers (Figure 5a), while broadband EQE are collected, the current selective peak at ~800 nm starts to be visible only for 972 nm thick layers. By increasing the thickness, this single peak predominates for ultra-thick blends (3310 nm) to deliver a narrow wavelength-selective photodetection. It must be mentioned that for 1903–2192 nm thick layers, even if a selective peak appears at 792 nm, the persistent presence of a spectral response between 300 and 750 nm does not make the devices highly selective OPDs according to the CCN principle. For annealed active layers at 200°C (Figure 5b), the emergence of the selective peak can already be observed for thin films (239 nm) to be only the detection part in the 1345 and 2740 nm thick layers. It has been particularly demonstrated for this blend a joint correlation between the induced increase in crystallinity of the ITIC-4F domains, charge carriers mobility and EQE profile as function of post-annealing temperature (100°C or 200°C).[3d]

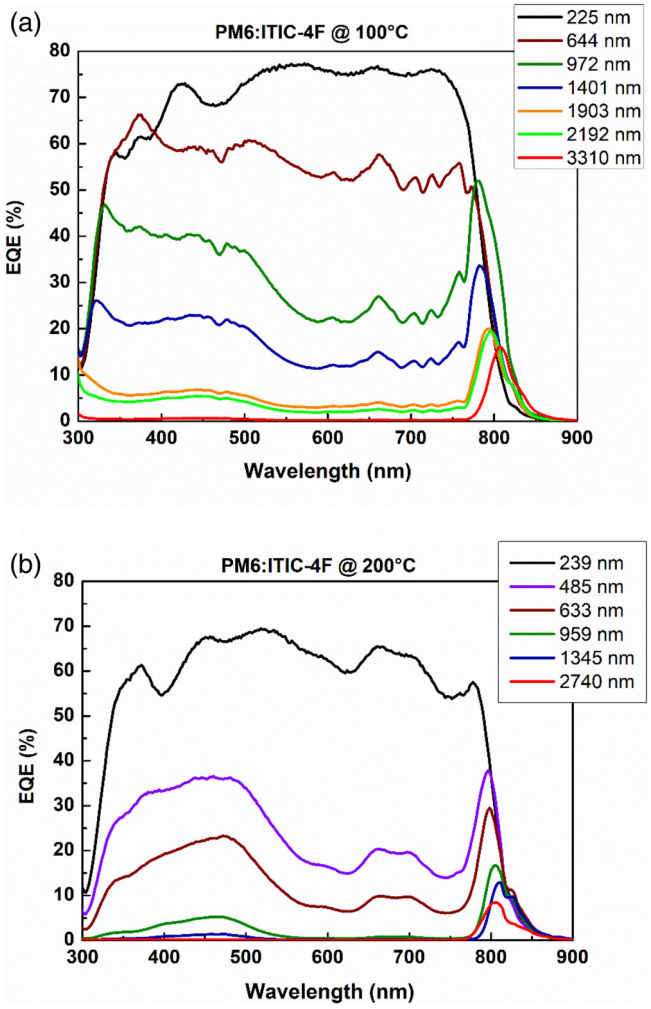

FIGURE 5 External quantum efficiency (EQE) spectra of OPDs as function of PBDB-T-2F:ITIC-4F thickness and post-annealing temperature: (a) 100°C and (b) 200°C. [Color figure can be viewed at wileyonlinelibrary.com]

Thickness and morphology control of the BHJ films have been validated to be crucial to achieve a narrowband response in OPDs.[2f,3a] Film morphology therefore plays a key role and can be analyzed by atomic force microscopy (AFM), contact water angle (CWA) measurement, Raman analyses, and 2D grazing-incidence x-ray diffractometry (2D-GIXRD). An ideal morphology should lead to a bi-continuous network free from large areas of phase separation or isolated aggregation. In the case of PBDB-T-2F:ITIC-4F based CCN-OPDs, we were able to demonstrate that it was possible to reduce the thickness of the layer, but at the counterpart of increasing its annealing temperature.[3d] However, for applications in industry and everyday life, PD-type OPDs based on the CCN concept have to overcome a number of constraints, such as an active organic layer thickness of less than 2 μm and post-deposition

10974628, 0, Downloaded from https://onlinelibrary.wiley.com/doi/10.1002/app.55481 by Cochrane France, Wiley Online Library on [23/03/2024]. See the Terms and Conditions (https://onlinelibrary.wiley.com/terms-and-conditions) on Wiley Online Library for rules of use; OA articles are governed by the applicable Creative Commons License

TABLE 1 Thickness and OPD parameters of devices at 0 V.

Blend	Thickness (μm)	λ_{target} (nm)	EQE (%)	FMWH (nm)	$\Re_{target}$ (mA.W^{-1})	$\Re_{untarget}$ (mA.W^{-1})	SRR
PBDB-T-2F:$PC_{70}BM$	1.6	674	19.26	43	104.6	0.55	190.2
PBDB-T: eh-IDTBR	1.1	730	7.88	41	46.3	10.55	4.4
F8T2:ITIC-Th	1.9	760	0.91	28	5.5	0.10	55
PBDB-T-2F:ITIC-4F	1.9	794	20	36.5	127.9	24.58	5.2

Note: λ_{target} corresponds to the wavelength of the selective peak and EQE to its value in % in non-normalized spectra. $\Re_{target}$ and $\Re_{untarget}$ are the calculated responsivity values with $\lambda_{untarget}$ = 460 nm for PBDB-T-2F:$PC_{70}BM$, PBDB-T: eh-IDTBR, PBDB-T-2F:ITIC-4F and 532 nm for F8T2:ITIC-Th.

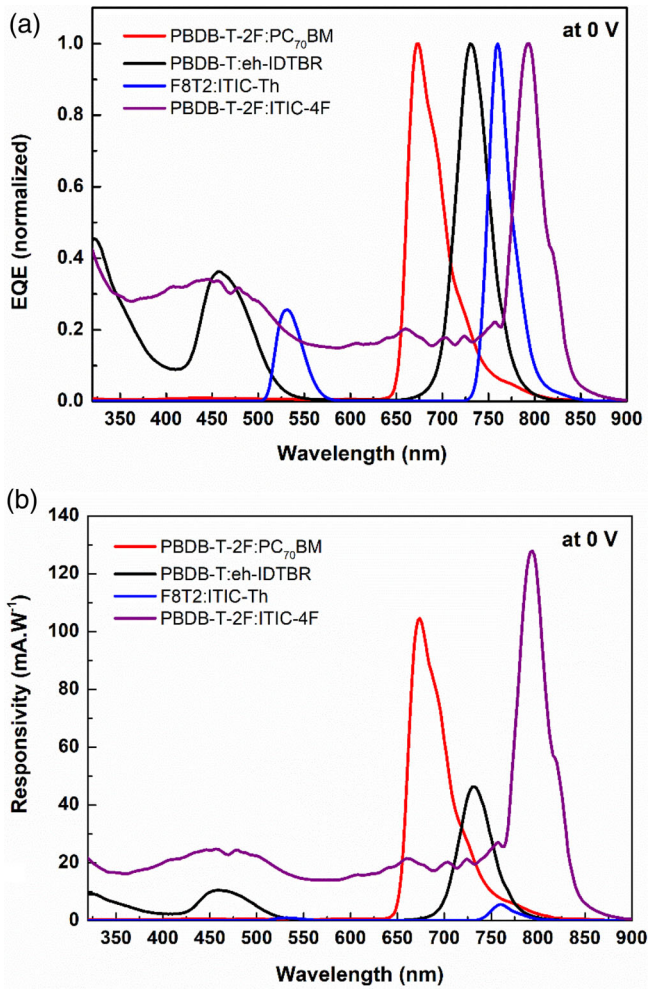

FIGURE 6 (a) Normalized external quantum efficiency (EQE) spectra of OPDs as function of BHJ composition (donor:acceptor BHJ in 1:1 w/w ratio, post-annealed at 100°C during 10 min, thickness < 2 μm). EQEs are recorded at an applied bias of 0 V. (b) Calculated corresponding responsivity spectra of OPDs from the EQE measurement. [Color figure can be viewed at wileyonlinelibrary.com]

annealing temperatures not in excess of 100°C. For these reasons, obtaining a BHJ that complies with its criteria is of prime importance.

3.3 | Dependence on organic materials for wavelength-selective photodetection

For further study of the dependence of OPDs on the organic materials used in BHJs, we realized OPDs based on PBDB-T-2F:$PC_{70}BM$, PBDB-T: eh-IDTBR and F8T2:ITIC-Th as BHJ layers in 1:1 weight ratio post-annealed at 100°C. All organic BHJ layers have a final thickness of less than 2 μm (Table 1). Figure 6a shows normalized EQE spectra at zero bias (0 V) of OPDs with selective peaks at λ_{target} equal to 674, 730, 760 and 794 nm for PBDB-T-2F:$PC_{70}BM$, PBDB-T: eh-IDTBR, F8T2:ITIC-Th and PBDB-T-2F:ITIC-4F, respectively. It is worth to note that these selective peaks appear at λ_{onset} of corresponding BHJ layer as predicted by the CCN principle. While only the PBDB-T-2F:$PC_{70}BM$ based OPD demonstrates an ideal blind property outside the detection peak, a secondary detection peak and/or a continuous residual detection is observed for the others. The specific nature of these differences will be discussed in section 3.4.

Figure 6b shows the calculated responsivity spectra from the EQE measurements (Figure S2) by using equation 1 where $\Re_{target}$ and $\Re_{untarget}$ are the calculated responsivity values at corresponding λ_{target} (wavelength at maximum responsibility) and $\lambda_{untarget}$ (460 nm for PBDB-T-2F:$PC_{70}BM$, PBDB-T: eh-IDTBR, PBDB-T-2F:ITIC-4F and 532 nm for F8T2:ITIC-Th). A maximum value $\Re_{target}$ of 127.9 mA.W^{-1} is reached for PBDB-T-2F:ITIC-4F based OPDs. By blending the PBDB-T-2F donor polymer with $PC_{70}BM$, a slight decrease in $\Re_{target}$ to 104.6 mA.W^{-1} is measured with however an extremely low $\Re_{untarget}$ leading to the highest SRR value with 190.2. Such high SSR value (> 100) is obtained uniquely for this $PC_{70}BM$ based blend. Indeed, with a continuous residual detection outside the selective peak, ITIC-4F based OPD has an extremely high $\Re_{untarget}$, reducing its SSR to 5.2. With really low $\Re_{target}$ and SRR values, PBDB-T: eh-IDTBR and F8T2:ITIC-Th based OPDs do not satisfy the criteria defined in this study to be classified as efficient narrowband CCN-OPDs. With a third very favorable parameter, that is, an extremely low FWHM (<50 nm),

10974628, 0, Downloaded from https://onlinelibrary.wiley.com/doi/10.1002/app.55481 by Cochrane France, Wiley Online Library on [23/03/2024]. See the Terms and Conditions (https://onlinelibrary.wiley.com/terms-and-conditions) on Wiley Online Library for rules of use; OA articles are governed by the applicable Creative Commons License

only PBDB-T-2F:$PC_{70}BM$ based OPDs fulfill the specifications for being high selective narrowband OPDs.

Moreover, the spectral selectivity of our narrowband CCN-OPD is based on the manipulation of free charge carriers after exciton dissociation.[3a] The effect of applied electric field on the photogenerated charge carrier collection is therefore not negligible. As a result, EQE values generally increase with reverse polarization.[2i,3f,6] Figure S3 shows measured and normalized EQE of OPDs based on PBDB-T-2F:$PC_{70}BM$, PBDB-T: eh-IDTBR, F8T2:ITIC-Th and PBDB-T-2F:ITIC-4F recorded at an applied bias of −2 V together with calculated corresponding responsivity spectra. Even though all OPDs recorded an increase in $\mathfrak{R}_{target}$, trends remain unchanged with $\mathfrak{R}$ reaches maximum values for PBDB-T based OPDs blended with ITIC-4F or $PC_{70}BM$. However, only OPDs based on PBDB-T-2F:$PC_{70}BM$ retain an acceptable SRR value to qualify the OPD as a filter-free band-selective OPD with high selectivity and responsivity.

The PBDB-T-2F donor polymer was blended with IO-4Cl as acceptor molecule to form a photo-active BHJ layer in OPDs. With a great absorption spectrum overlap between IO-4Cl and PBDB-T-2F absorption spectra (Figure 3e), the selective peak may not be extended to near-IR wavelengths, as in the case of ITIC-4F. In this case, λ_{target} (686 nm) value is very close to λ_{onset} of PBDB-T-2F (677 nm) and IO-4Cl (680 nm). Figure S4 shows EQE spectra at 0 V and at −2 V of PBDB-T-2F:IO-4Cl based OPDs with those based on PBDB-T-2F:$PC_{70}BM$. Despite the emergence of a single selective peak, extremely low $\mathfrak{R}_{target}$ (0.10 mA W^{-1} at 0 V and 0.31 mA W^{-1} at −2 V) are calculated (Figure S5 and Table S3).

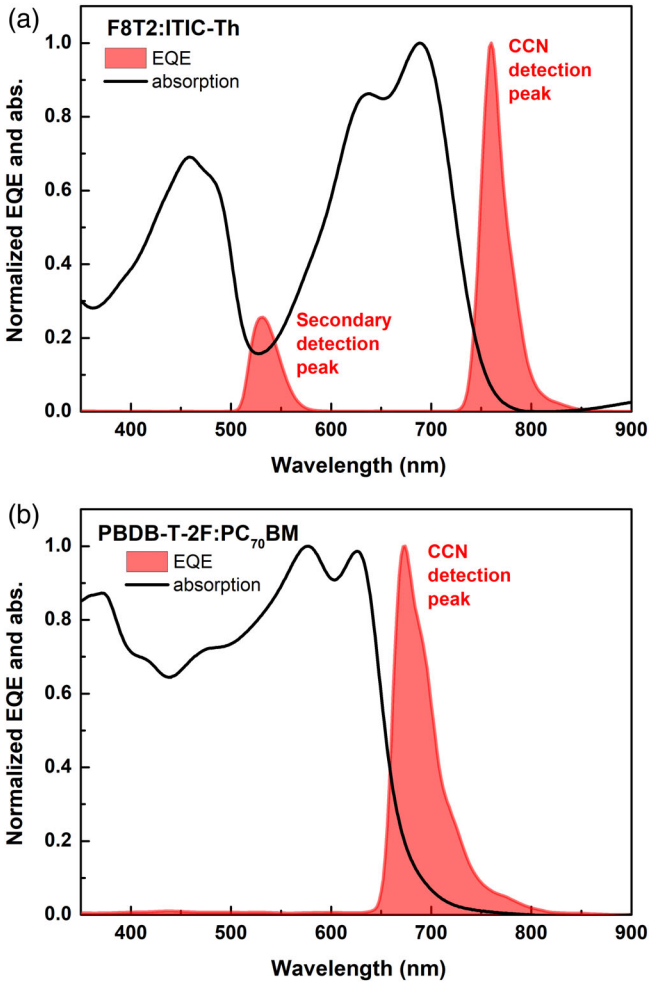

FIGURE 7 Normalized external quantum efficiency (EQE) spectra of OPDs and corresponding BHJ absorption spectra for F8T2:ITIC-Th (a) and PBDB-T-2F:$PC_{70}BM$ (b). [Color figure can be viewed at wileyonlinelibrary.com]

3.4 | Correlation between absorption spectra and EQE profile in CCN principle

If only OPDs based on the PBDB-T-2F:$PC_{70}BM$ satisfy the requirements of highly efficient narrowband CCN-OPDs, that is, high EQE value, low FMWH and high SRR value, it is worth highlighting the direct correlation between EQE and absorption spectra. Figure 7 shows the normalized EQE spectra of OPDs and corresponding BHJ absorption spectra for F8T2:ITIC-Th and PBDB-T-2F:$PC_{70}BM$. In the case of F8T2:ITIC-Th, even though the absorption spectrum of the blend corresponds to the addition of the two spectra of single layers, a very low absorption minimum appears at 528 nm (Figure 7a). With a relative absorbance of 0.18 compared with the absorption maximum, this minimum is 82% less absorbing than the maximum peak. Consequently, photons whose energy corresponds to the absorption minimum will be absorbed intensely in the active layer to generate light carriers. In the EQE spectrum, this translates into a specific photoresponse at 530 nm in the form of a secondary detection peak. The CCN detection peak and the secondary detection peak appear on either side of the main absorption band. To suppress the EQE response of the secondary detection peak, a third organic materials can be introduced to cover the dip area of the blend absorption spectrum.[2f] However, by adding a third compound, the ink preparation will require its own optimisation, that is, determination of the ratio between the three compounds, the final concentration and the deposition conditions, resulting in additional steps. Moreover, this third compound must not generate unfavorable phase separation domains or isolated aggregation.

On the contrary, the absorption spectrum of PBDB-T-2F:$PC_{70}BM$ blend shows no pronounced minima with a relative absorbance never lower than 35.5% of the maximum peak (Figure 7b). The relative absorption range is

10974628, 0, Downloaded from https://onlinelibrary.wiley.com/doi/10.1002/app.55481 by Cochrane France, Wiley Online Library on [23/03/2024]. See the Terms and Conditions (https://onlinelibrary.wiley.com/terms-and-conditions) on Wiley Online Library for rules of use; OA articles are governed by the applicable Creative Commons License

always greater than 60% outside the absorption tail rendering the layer opaque, or blind, to these wavelengths. In this case, photons whose energy corresponds to the absorption peak of materials will be absorbed, according to the Beer–Lambert law, near the illuminated surface of the active layer where photo-carrier generation will occur. Due to the low charge mobility and thickness of active layer, the generated charges tend to recombine before reaching the back electrodes.[3e] In contrast, photons with energy close to the absorption tail can penetrate further into active layer and charges can be generated uniformly across the thick film. Thus, an EQE response is obtained at the wavelength near the absorption tail. This is ideally reflected in the EQE spectrum by a CCN detection peak and blindness outside this spectral window.

The identical comparison for PBDB-T: eh-IDTBR, PBDB-T-2F:IO-4Cl and PBDB-T-2F:ITIC-4F are depicted in Figure S6. All EQE profiles exhibit more or less pronounced residual detection generally observed between the two detection peaks, as in the case of PBDB-T-2F:ITIC-4F. This undesirable detection can generally be eliminated by increasing layer thickness (towards ultra-thick layer, thickness $\gg 2\,\mu m$), but at the expense of CCN peak intensity. Therefore, narrowband OPDs with the desired peak response, high EQE and SRR can be expected by selecting donor and acceptor materials to match the initial prerequisites such as not too thick layers deposited by the solution deposition process and an annealing temperature not exceeding 100°C.

4 | CONCLUSION

Here we design simple and readily accessible device architectures to achieve spectral selectivity through the CCN principle. BHJs based on the mixture between donor polymer and electron acceptor at 1:1 weight ratio have been deposited as an active layer in OPD using a solution process. Five different BHJs as PBDB-T-2F:$PC_{70}BM$, PBDB-T: eh-IDTBR, F8T2:ITIC-Th, PBDB-T-2F:ITIC-4F and PBDB-T-2F:IO-4Cl were selected. We examine relevant trends, highlighting the direct correlation between BHJ absorption range and EQE profile to assist in the development of a selective detection peak with layer thickness of less than 2 μm and post-deposition annealing temperatures not in excess of 100°C. The PBDB-T-2F:$PC_{70}BM$ blend stands out by an absorption spectrum corresponding to the addition of the two spectra of single layers and covering a wide UV–Visible range. The most important point is that there are no pronounced absorption minima making the layer opaque between 350 and 750 nm. PBDB-T-2F:$PC_{70}BM$ based OPD therefore demonstrates an ideal CCN-behavior with a single-peak EQE response of 20% at a centered wavelength at 675 nm along with a narrow FWHM of less than 50 nm and a SRR greater than 100. It should be noted that, different from the response peak which is highly dependent on the absorption spectra of donor and acceptor, the EQE and SRR values are affected by the photon-electron conversion efficiency of donor and acceptor combination. Additionally to overcome the constraints associated with their use applied devices, PD-type OPDs based on the CCN concept require an active organic layer thickness of less than 2 μm and post-deposition annealing temperatures not in excess of 100°C. We show here that it is not obvious to combine the efficiency parameters while avoiding the constraints of thickness and annealing temperature of organic layers. Therefore, such narrowband OPDs can be expected by selecting existing donor and acceptor materials, or designing new materials.

AUTHOR CONTRIBUTIONS

Quentin Eynaud: Conceptualization (equal); methodology (equal). **Anass Khodr:** Methodology (supporting). **Mohamed El Amine Kramdi:** Conceptualization (supporting). **Gilles Quéléver:** Conceptualization (supporting). **Olivier Margeat:** Methodology (supporting); resources (supporting). **Jörg Ackermann:** Conceptualization (supporting); funding acquisition (equal); investigation (supporting). **Christine Videlot-Ackermann:** Methodology (equal); supervision (lead); writing – original draft (lead).

ACKNOWLEDGMENTS

This project has received funding by the French Research Agency (project ANR-18-CE04-0007-04 named BELUGA and project ANR-22-CE06-0018 named MONOPOLY). C.V.A. and J.A thank F. Jandard and S. Lavandier from CINaM (Electronics and instrumentation division) for their assistance in building the OPD measurement facilities and developing the acquisition software.

DATA AVAILABILITY STATEMENT

The authors confirm that the data supporting the findings of this study are available within the article and its supplementary materials.

ORCID

Quentin Eynaud https://orcid.org/0009-0009-1871-9455
Anass Khodr https://orcid.org/0000-0002-8521-7641
Mohamed El Amine Kramdi https://orcid.org/0000-0002-1967-9207
Gilles Quéléver https://orcid.org/0000-0002-3738-6109
Olivier Margeat https://orcid.org/0000-0003-3716-2399
Jörg Ackermann https://orcid.org/0000-0003-2586-3788
Christine Videlot-Ackermann https://orcid.org/0000-0001-8240-6474

10974628, 0, Downloaded from https://onlinelibrary.wiley.com/doi/10.1002/app.55481 by Cochrane France, Wiley Online Library on [23/03/2024]. See the Terms and Conditions (https://onlinelibrary.wiley.com/terms-and-conditions) on Wiley Online Library for rules of use; OA articles are governed by the applicable Creative Commons License

REFERENCES

[1] (a) J. H. Kim, A. Liess, M. Stolte, A.-M. Krause, V. Stepanenko, C. Zhong, D. Bialas, F. Spano, F. Würthner, *Adv. Mater.* **2021**, *33*, 2100582. (b) Z. J. Lan, M. H. Lee, F. R. Zhu, *Adv. Intell. Syst.* **2022**, *4*, 2100167. (c) Y. Z. Wang, J. Kublitski, S. Xing, F. Dollinger, D. Spoltore, J. Benduhn, K. Leo, *Mater. Horiz.* **2022**, *9*, 220.

[2] (a) W. B. Wang, F. J. Zhang, M. D. Du, L. L. Li, M. Zhang, K. Wang, Y. S. Wang, B. Hu, Y. Fang, J. S. Huang, *Nano Lett.* **2017**, *17*, 1995. (b) J. Miao, F. Zhang, M. Du, W. Wang, Y. Fang, *Phys. Chem. Chem. Phys.* **2017**, *19*, 14424. (c) J. Miao, F. Zhang, M. Du, W. Wang, Y. Fang, *Adv. Optical Mater.* **2018**, *6*, 1800001. d) W. Wang, M. Du, M. Zhang, J. Miao, Y. Fang, F. Zhang, *Adv. Optical Mater.* **2018**, *6*, 1800249. (e) Z. Zhao, C. Xu, Y. Ma, X. Ma, X. Zhu, L. Niu, L. Shen, Z. Zhou, F. Zhang, *Adv. Funct. Mater.* **2023**, *33*, 2212149. (f) B. M. Xie, R. H. Xie, K. Zhang, Q. W. Yin, Z. C. Hu, G. Yu, F. Huang, Y. Cao, *Nat. Commun.* **2020**, *11*, 2871. (g) K. M. Sim, S. Yoon, J. Cho, M. S. Jang, D. S. Chung, *ACS Appl. Mater. Interfaces* **2018**, *10*, 8405. (h) J. Kim, S. Yoon, K. M. Sim, D. S. Chung, *J. Mater. Chem. C* **2019**, *7*, 4770. (i) Z. J. Lan, Y. S. Lau, Y. W. Wang, Z. Xiao, L. M. Ding, D. Luo, F. R. Zhu, *Adv. Opt. Mater.* **2020**, *8*, 20001308.

[3] (a) A. Armin, R. D. J.-v. Vuuren, N. Kopidakis, P. L. Burn, P. Meredith, *Nat. Commun.* **2015**, *6*, 6343. (b) A. Armin, A. Yazmaciyan, M. Hambsch, J. Li, P. L. Burn, P. Meredith, *ACS Photonics* **2015**, *2*, 1745. c)A. Yazmaciyan, P. Meredith, A. Armin, *Adv. Optical Mater.* **2019**, *7*, 1801543. (d) Q. Eynaud, Y. A. A. Quiroz, T. Koganezawa, R. Sato, N. Yoshimoto, O. Margeat, C. M. Ruiz, J. Ackermann, C. Videlot-Ackermann, *J. Mater. Chem. C* **2023**, *11*, 9657. (e) Q. Eynaud, M. el Amine Kramdi, V. Kannampalli, T. Koganezawa, N. Yoshimoto, L. Santinacci, J. Ackermann, C. Videlot-Ackermann, *Adv. Energy Sustain. Res.* **2024**, 2300262. (f) K. W. Tsai, G. Madhaiyan, L. H. Lai, Y. T. Hsiao, J. L. Wu, C. Y. Liao, C. H. Hou, J. J. Shyue, *ACS Appl. Mater. Interfaces* **2022**, *14*, 38004.

[4] S. Ben Dkhil, M. Pfannmöller, R. R. Schröder, R. Alkarsifi, M. Gaceur, W. Köntges, H. Heidari, S. Bals, O. Margeat, J. Ackermann, C. Videlot-Ackermann, *ACS Appl. Mater. Interfaces* **2018**, *10*, 3874.

[5] M. Kielar, O. Dhez, G. Pecastaings, A. Curutchet, L. Hirsch, *Sci. Rep.* **2016**, *6*, 39201.

[6] H. Bristow, P. Jacoutot, A. D. Scaccabarozzi, M. Babics, M. Moser, A. Wadsworth, T. D. Anthopoulos, A. Bakulin, I. McCulloch, N. Gasparini, *ACS Appl. Mater. Interfaces* **2020**, *12*, 48836.

SUPPORTING INFORMATION

Additional supporting information can be found online in the Supporting Information section at the end of this article.

How to cite this article: Q. Eynaud, A. Khodr, M. E. A. Kramdi, G. Quéléver, O. Margeat, J. Ackermann, C. Videlot-Ackermann, *J. Appl. Polym. Sci.* **2024**, e55481. https://doi.org/10.1002/app.55481

10974628, 0, Downloaded from https://onlinelibrary.wiley.com/doi/10.1002/app.55481 by Cochrane France, Wiley Online Library on [23/03/2024]. See the Terms and Conditions (https://onlinelibrary.wiley.com/terms-and-conditions) on Wiley Online Library for rules of use; OA articles are governed by the applicable Creative Commons License